Hindawi Publishing Corporation
Advances in Mathematical Physics
Volume 2010, Article ID 482598, 21 pages
doi:10.1155/2010/482598

Review Article

Cluster State Computation with Quantum-Dot Charge Qubits

Matthew Lubelski Katz and Jingbo Wang

School of Physics, The University of Western Australia, Perth, WA 6009, Australia

Correspondence should be addressed to Jingbo Wang, wang@physics.uwa.edu.au

Received 14 July 2009; Accepted 15 October 2009

Academic Editor: Shao-Ming Fei

Quantum computers are expected to far surpass the capabilities of today's most powerful supercomputers, particularly in areas such as the theoretical simulation of quantum systems, cryptography, and information processing. The cluster state is a special, highly entangled quantum state that forms the universal resource on which measurement-based quantum computation can be performed. This paper provides a brief review of the theoretical foundations of cluster state quantum computation and how it evolved from the traditional model of digital computers. It then proposes a scheme for the generation of such entanglement in a solid-state medium through the suppression of resonant tunneling of a ballistic electron by a single-electron charge qubit. To investigate the viability of the scheme for the creation of cluster states, numerical calculations are performed in which the entanglement interaction is modeled in detail.

1. Introduction

The simulation of quantum systems is an integral part of modern science. Such simulations are difficult, however, due to the massive computational resources they require. Quantum computers [1] offer a unique solution to this problem by explicitly using quantum mechanics to perform computation more efficiently. While they promise much, building practical quantum computers using implementations analogous to those of digital computing has proved extremely challenging. In 2001, Raussendorf and Briegel [2] proposed a more robust implementation that used a highly entangled *cluster state* as a universal resource on which to perform measurement-based quantum computation. The systematic generation of entanglement suitable for the creation of such cluster states is consequently of great importance in the realization of a viable quantum computer.

We begin this paper by giving a brief review of the theoretical foundations of cluster state quantum computation and how it evolved from the traditional model of digital

computers. In the next section, we outline a scheme to generate controlled entanglement in a solid-state system using resonant tunneling and give details of the simulation and numerical techniques used to test it. In Section 3, we present the results from our simulation and, in Section 4, discuss the possible difficulties of using such a scheme to generate a cluster state.

1.1. Computation and Physical Simulations

It was Turing, in his revolutionary 1936 paper "On Computable Numbers, with an Application to the Entscheidungsproblem" [3], who first proposed the computational model used by all modern computers. He showed that any mathematical operation with an arithmetic formulation, called a *computable function*, could be performed with finite means by a simple physical device. This theoretical device, known as the *universal Turing machine*, used a set of basic mechanical actions to manipulate symbols on an infinite one-dimensional paper tape. During each step of computation, the machine would address only a single symbol on the tape and perform a single action that depended on the symbol's value and the machine's variable internal state. The particular action taken at each step was controlled by an internal table of conditional instructions, called an *algorithm*. By constructing a suitable algorithm, such a machine could be made to automatically perform any arithmetic operation on numbers encoded on the tape using only a finite number of steps. What made the universal Turing machine so powerful was that a small set of basic actions, symbols, and instructions could be used with only local information about the system to perform all arithmetic operations in a finite time. While constructing such a mechanical device proved impractical, Turing's model formed the template for all modern computers.

Unlike the universal Turing machine, a modern computer is a digital device based on the laws of electrodynamics. In place of paper tape, computers use binary digits, called *bits*, to store and process information. Physically, bits are addressable electronic systems that can have only one of two possible computational states labeled 0 and 1. Information, known as *input*, is encoded onto a number of bits via some binary discretizing schema. Computation is then performed by sequentially switching the bits between their 0 and 1 states using simple one- and two-bit operations called *Boolean logic gates*. The final state of the bits is then read off and decoded to give the result, or *output*, of the computation. While this implementation appears significantly different from Turing's, a set of just two two-bit Boolean logic gates, the *universal gates* NAND and NOR, can perform all binary boolean algebraic operations using only finite means. This allows a digital computer to deterministically transform a set of input bits into any possible output and so act as a universal Turing machine.

It is the universality of digital computers that has made them such an invaluable tool in modern life and enabled complex simulations of physical systems to be performed. This has led scientists to ask an important question: "what kind of physical systems can be efficiently simulated on a digital computer?" Turing envisaged his universal machine performing computations using an infinite paper tape over some finite, but arbitrarily long, amount of time. As infinite computational resources are impossible, the efficiency with which a computer uses its resources and the time a computation takes to complete impose a physical limit on what can and can not be "reasonably" simulated. This constraint, called *tractability*, can be formalized by demanding that the number of bits and gate operations of a digital computation scales polynomially with the complexity of the system being simulated. Unfortunately for physicists, the simulation of systems governed by the laws of quantum mechanics is generally intractable and so cannot be efficiently performed using

digital computers. This becomes apparent by considering that the size of the Hilbert space characterizing a quantum system grows exponentially with the number of particles in it. For example, to simulate a system of only 500 spin 1/2 particles a digital computer must posses enough bits to represent 2^{500} complex numbers just to describe its general state.

1.2. Quantum Computation

It was the question of efficiency, and in particular the intractability of simulating quantum systems, that lead Feynman in 1982 [4] to propose a model for a universal quantum simulator. He realized that the inefficiency of digital computers in simulating quantum systems was due to the underlying electrodynamic laws used in their implementation. Feynman argued that by basing a computer explicitly on the laws of quantum mechanics more efficient simulations could be performed. In 1985, Deutsch [1] took the final step in defining a model of quantum computation by combining Feynman's simulator with the universal Turing machine and showed it was possible to construct a *universal quantum Turing machine* that could perform these simulations using only finite means. This machine was not only truly universal but possessed unique quantum properties that allowed it to compute certain problems more efficiently.

One of the defining features of quantum computation is *quantum parallelism*. As a quantum system can exist in a linear superposition of its basis states, the universal quantum Turing machine can, at any step in the computation, represent *all* possible computational states simultaneously. If this superposition is preserved, then by applying suitable unitary operators to the system it can, in a *single step*, perform a computation on all these states that scales exponentially with the required physical resources. This would be equivalent to running computation on massively paralleled digital computers; however such a simple comparison is deceptive as to obtain classical output from the quantum system it must first be measured. When this measurement is performed, the system randomly collapses into one of its basis states destroying the superposition. This means that quantum computation is probabilistic. Only by designing algorithms that take advantage of interference effects the probability of a particular result can be made arbitrarily high and so deterministic computations performed. Useful quantum algorithms have already been designed for solving, as yet, intractable problems such as the factoring of large numbers [5] and list searching [6]. These algorithms, as well as efficient simulation of quantum systems, mean that a practical quantum computer would be hugely beneficial to modern science.

1.2.1. The Qubit

To construct a quantum computer, input must first be encoded onto a logical unit that can be manipulated in the required manner during computation. The quantum binary digit, or *qubit*, is the simplest form such a unit can take and is a natural extension of the digital bit. A qubit, like a bit, is an addressable two-level system with two discrete observable orthonormal basis states labeled $|0\rangle$ and $|1\rangle$. Qubits, however, are explicitly quantum systems and so their general state is described by the two-dimensional Hilbert space $\mathscr{H}$ spanned by the orthonormal basis states of these observables. The general pure state of the qubit $|\Psi\rangle$ can consequently be described by the linear superposition

$$|\Psi\rangle = c_0|0\rangle + c_1|1\rangle \tag{1.1}$$

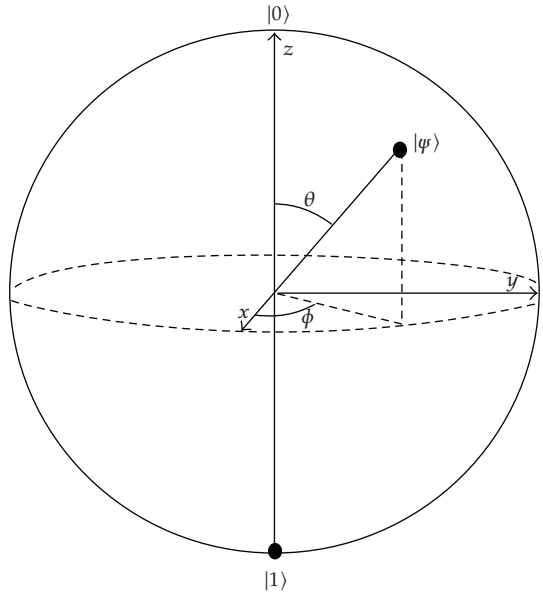

Figure 1: The Bloch Sphere—a geometric representation of the Hilbert space of a qubit. Any pure qubit state, modulo a global phase, can be represented by a point on the surface of the sphere given by $|\Psi\rangle = \cos\theta|0\rangle + e^{\imath\phi}\sin\theta|1\rangle$.

with $c_0, c_1 \in \mathbb{C}$ and $|c_0|^2 + |c_1|^2 = 1$ for normalization. The probability of measuring the qubit in the $|0\rangle$ or $|1\rangle$ state is then given by $|c_0|^2$ and $|c_1|^2$, respectively. A useful geometric representation of the qubits Hilbert space can be constructed by re-parameterizing the general state as

$$|\Psi\rangle = \cos\theta|0\rangle + e^{\imath\phi}\sin\theta|1\rangle, \tag{1.2}$$

where θ and ϕ are angles that correspond to a point on an S^2 sphere, known as the Bloch sphere (shown in Figure 1).

As the state of a single qubit, modulo a global phase, must always reside on the Bloch Sphere, the action of any single-qubit unitary operation $W \in SU(2)$ can be represented by the set of Euler rotations:

$$W|\Psi\rangle = X(\alpha)Z(\theta)X(\beta)|\Psi\rangle, \tag{1.3}$$

where α, θ, and β are real valued and $X(\alpha)$ and $Z(\theta)$ are rotations about the x- and z-axis of the Bloch sphere, respectively. An arbitrary single-qubit unitary operation $U \in U(2)$ can then be written as $U = e^{\imath\delta}W$ where δ is a real valued global phase shift.

To perform quantum computation a number of qubits N must be acted upon by a series of unitary evolution operators $U \in U(2^N)$ that affect some predetermined action. The computational Hilbert space is thus formed by the space of all possible qubit states and is spanned by the orthonormal basis states $|\phi\rangle$ given by the tensor products:

$$|\phi\rangle = |\varphi\rangle_1 \otimes |\varphi\rangle_2 \otimes \cdots \otimes |\varphi\rangle_N \in \mathcal{H}^{\otimes N}, \tag{1.4}$$

where $|\psi\rangle_i \in \{|0\rangle, |1\rangle\}_i$ is the basis state of the ith qubit. By using a superposition of these states a quantum computer can represent multiple sequences of classical bits simultaneously giving rise to quantum parallelism.

1.2.2. The Quantum Circuit Model

Due to its similarity with traditional digital circuits, the most widely used representation of quantum computation is the *quantum circuit model*. In this model, a sequence of noninteracting qubits, called the quantum register, is first prepared in the desired input state. Computation is then performed by sequentially applying one- and two-qubit unitary operations, called *quantum logic gates*, before the qubits are measured to obtain the output. Just as Boolean logic circuits can be shown to be equivalent to the universal Turing machine, such quantum circuits have been shown to be equivalent to the universal quantum Turing machine [7].

An important example of a quantum circuit is the single-qubit "teleporter" which is represented by the following circuit diagram:

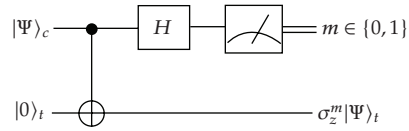

In quantum circuit diagrams, time flows from left to right with the horizontal lines, called *quantum wires*, representing the separate qubits that comprise the quantum register. One-qubit operations and gates are represented on single quantum wires and two-qubit gates are represented by using perpendicular lines to show interaction, and so entanglement, between the relevant qubits. The "teleporter" circuit functions by first entangling the control qubit (top wire) with a target qubit prepared in the $|0\rangle$ state (bottom wire) using the two-qubit CNOT gate. This applies a NOT operation to the target-qubit if and only if the control-qubit is in the $|1\rangle$ state. Once entangled, the control-qubit passes through a single-qubit Hadamard gate and its observable state is measured. The resulting state of the target-qubit will then be $\sigma_z^m|\Psi\rangle_t$, where $m \in \{0,1\}$ is the outcome of the measurement on the control-qubit. This circuit is called the single-qubit "teleporter" as the state of the control-qubit is "teleported," with a possible additional factor σ_z (the Pauli spin matrix), to the target-qubit via their entanglement.

It is a remarkable property of the quantum circuit model that any unitary evolution operator needed for quantum computation can be perfectly simulated using only two-qubit gates $\{U_2 : U_2 \in U(2^2)\}$ [8]. This can be further simplified into just the two-qubit CNOT gate and the set of single-qubit gates $\{U_1 : U_1 \in U(2)\}$ [9] with which all two-qubit gates can be simulated. While these are truly *universal quantum gates*, allowing for the *exact* simulation of any unitary evolution operator, it is often more convenient to work with sets of gates that are only *approximately* universal. An approximately universal set of gates can efficiently simulate, to an arbitrary accuracy, any unitary evolution operator. One such set of *approximately universal quantum gates* is formed by only three gates $\{H, W = e^{\pi/8}Z(-\pi/8), \text{CNOT}\}$ [10].

The universality, both exact and approximate, of one- and two-qubit gates makes the quantum circuit model a powerful tool for the design and analysis of quantum algorithms. Practically, however, efficient physical implementations of the model have proved difficult to construct. Problems arise due to the need for both fault tolerant multiqubit gates and robust scalable qubits within a single system. For systems with strongly interacting qubits, multiqubit gates are more easily constructed; however, the qubits tend to experience

high levels of decoherence making them less robust. Conversely, for systems with weakly interacting qubits, the qubits are more robust but multiqubit gates are much harder to construct. This has lead physicists to consider a new model of quantum computation that can be more easily implemented—the cluster state or one-way computation model.

1.2.3. The Cluster State

The cluster state model for quantum computation was proposed by Raussendorf and Briegel in 2001 [2] as a scheme for performing quantum computing based on entanglement. Their model consisted of an ensemble of entangled qubits, known as the *cluster state*, on which computation and readout is performed by an adaptive sequence of single-qubit measurements. These measurements propagate quantum correlations through the system and, by combining their results via some tractable classical computation, generate the output. As measuring the individual qubits removes their entanglement and so destroys the original state, cluster state computation is also referred to as one-way computation. The great advantage of a cluster state computer is that in requiring only single qubit measurements it avoids many of the practical problems associated with the quantum circuit implementation.

The physical resource of cluster state computation is the titular "cluster state," which is a family of states of entangled qubits that can be defined by some graph $G(V, E)$. In this formulation, the vertices V of the graph represent the individual qubits and the edges E their entanglement. Conventionally, the term "cluster state" has been used to describe the specific class of graph states representing two-dimensional square lattices of qubits and this convention is followed here. To form the cluster, a collection of qubits is initially prepared in a maximally mixed pure state $|+\rangle \equiv (|0\rangle + |1\rangle)/\sqrt{2}$. Pairs of nearest neighbor qubits are then entangled using the two-qubit controlled phase gate:

$$\mathrm{CZ} = \begin{pmatrix} 1 & 0 & 0 & 0 \\ 0 & 1 & 0 & 0 \\ 0 & 0 & 1 & 0 \\ 0 & 0 & 0 & -1 \end{pmatrix}. \tag{1.5}$$

While the CZ gate has been used here for simplicity, it is a sufficient condition for the formation of the cluster state that nearest neighbor qubits be maximally entangled. Once the cluster has been formed, computation is performed by a series of adaptive single-qubit measurements in the variable basis

$$\mathcal{B}(\eta) = \left(\frac{|0\rangle + e^{-\imath\eta}|1\rangle}{\sqrt{2}}, \frac{|0\rangle - e^{-\imath\eta}|1\rangle}{\sqrt{2}} \right). \tag{1.6}$$

These measurements occur in sequential rounds with measurements in the same round being made simultaneously and those in later rounds being altered based on previous results. All the measurement results are then combined via a classical computation to generate the final output.

Recall that a single-qubit rotation $W \in SU(2)$ can be represented by

$$\begin{aligned} W|\Psi\rangle &= X(\alpha)Z(\theta)X(\beta)|\Psi\rangle \\ &= HZ(\alpha)HZ(\theta)HZ(\beta)HZ(0)|\Psi\rangle, \end{aligned} \tag{1.7}$$

where H is the Hadamard operator and the identities $X(\theta) = HZ(\theta)H$ and $Z(0) = I$ are used. To implement each of these four $HZ(\gamma)$ operations, the single-qubit "teleporter" circuit is modified to give

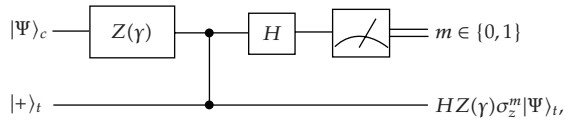

where the CNOT gate has been replaced by the CZ gate using the relation $\mathrm{CZ} = (I_c \otimes H_t)\mathrm{CNOT}(I_c \otimes H_t)$ and the additional Hadamard gates have been absorbed by the initial and final state of the target qubit ($|+\rangle = H|0\rangle$). As the $Z(\gamma)$ gate commutes with the CZ gate, the H and $Z(\gamma)$ gates can be combined and four of these circuits concatenated to give

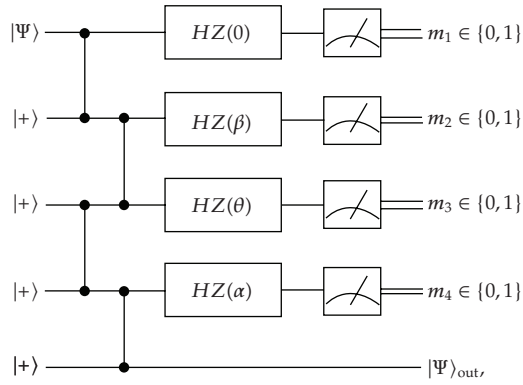

where

$$\begin{aligned} |\Psi\rangle_{\mathrm{out}} = {} & HZ(\alpha)\sigma_z^{m_4}HZ(\theta)\sigma_z^{m_3} \\ & \times HZ(\beta)\sigma_z^{m_2}HZ(0)\sigma_z^{m_1}|\Psi\rangle. \end{aligned} \tag{1.8}$$

Commuting the Pauli operators through the gate operations gives

$$\begin{aligned} |\Psi\rangle_{\mathrm{out}} = {} & \sigma_x^{m_4}\sigma_z^{m_3}\sigma_x^{m_2}\sigma_z^{m_1} \\ & \times HZ\left((-1)^{m_1+m_3}\alpha\right)HZ\left((-1)^{m_2}\theta\right) \\ & \times HZ\left((-1)^{m_1}\beta\right)HZ(0)|\Psi\rangle, \end{aligned} \tag{1.9}$$

which, ignoring the Pauli matrices and re-parameterizing, is a single-qubit rotation (see (1.7)) as desired. As an $HZ(\gamma)$ gate followed by a measurement of the computational basis is equal, up to a global phase, to a single-qubit measurement in the $\mathcal{B}(\gamma)$ basis, the conjugated circuit

is equivalent to the cluster state represented by the following graph:

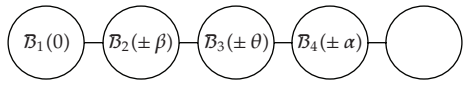

where the measurement basis is given in each vertex and the measurement round denoted by the subscript. By adapting the sign of the rotations based on the results of the previous measurements and compensating for any prefactor using a classical computation, an operation equivalent, modulo a global phase, to any single-qubit rotation $W \in SU(2)$ can be performed. In a similar manner it is possible to show that the CNOT gate can also be constructed [11] and so cluster state computation is computationally equivalent to the quantum circuit model where both inputs and outputs are classical.

The cluster state model of quantum computation offers a unique way of designing quantum algorithms. More than this, it provides a robust scheme for implementing a practical computing device. Such a device does not suffer from many of the disadvantages associated with a quantum circuit implementation as it uses only single qubit measurements to perform computation. Furthermore, it has been shown that a cluster state quantum computer would be more resilient to decoherence effects [12], can function efficiently even with only probabilistic entanglement [13], and provides the ability for efficient error correction [14, 15]. Before cluster state computation can be practically implemented, the controlled generation of entanglement necessary for the formation of the cluster state must be realized and this is the focus of this work.

2. Physical Implementation and Simulation

Multiqubit entanglement forms the universal resource on which all cluster state quantum computation is performed. To date, many physical systems have been proposed for the generation of such states including photons [16], cavity quantum electrodynamics [17], ions [18], optical lattices [19], and superconducting quantum circuits [20]. Schemes for generating cluster states in solid-state coupled double quantum dots (DQD) have also been proposed [21–23] and such a scheme is the focus here. A solid-state implementation is desirable for several key reasons; DQDs are highly scalable, allow for good control of charge and spin characteristics, and can have large spatial separations between qubits. Practically, a solid-state implementation would also benefit from the current expertise of the semiconductor industry.

In this paper, we present a detailed analysis on the entanglement generated between a single-electron charge qubit and a ballistic electron based on resonant tunneling. The modeled system consists of a charge qubit formed by a single-electron confined to a GaAs DQD. A GaAs quantum wire containing symmetric rectangular resonant tunneling barriers, formed by InAs slices, is positioned near to the centre of one of the dots and a ballistic electron pumped through the wire by a single-electron source [24]. The computational basis states of the qubit are then defined by the localization of the qubit electron to one of the two quantum dots with the state $|1\rangle$ corresponding to that closest to the quantum wire. A schematic diagram of this scheme is shown in Figure 2. By numerically simulating the system in detail, rather than assuming a simple interaction based on Pauli operators, a realistic determination of the systems suitability for cluster state generation can be made.

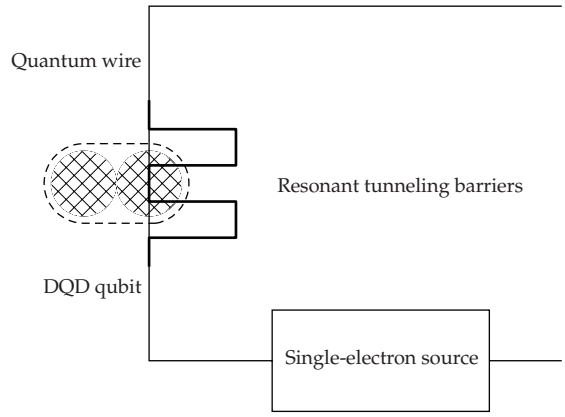

Figure 2: A schematic diagram of the system for generating entanglement between a ballistic electron and double quantum dot (DQD) single-electron charge qubit. The ballistic electron is pumped through the resonant tunneling barriers in the quantum wire by a single-electron source. Resonant tunneling occurs when the qubit electron is localized to the dot furthest from the wire, the $|0\rangle$ state, and is suppressed by Coulombic interaction when the qubit electron is localized to the dot closest to the wire, the $|1\rangle$ state.

2.1. Approximations

Both the qubit and quantum wire being modeled are confined to the conduction band of a GaAs semiconductor heterostructure. Lattice and screening effects are accounted for by using a linear approximation for the effective electron mass and permittivity of $m^* = 0.0667 m_e$ and $\epsilon = 12.9\epsilon_0$ [25], respectively. Throughout the simulation, the ballistic and qubit electrons are well separated in space and so distinguishable. Consequently, only Coulombic interactions between the electrons are modeled with spin-orbit and spin-spin coupling effects considered negligible in comparison. Decoherence and thermal effects are also ignored as, to a first approximation, the system is considered to be well isolated from the environment and operating in the low-temperature regime. The total system is then completely described by a Hamiltonian composed of the kinetic energy operators of both electrons, the Coulombic interaction between them, the potential of the resonant tunneling barriers experienced by the ballistic electron, and the confinement potential for the electron in the qubit. As the electron energies being considered are small ($E \ll m_e c^2 = 0.511\,\text{MeV}$) and only light elements (GaAs) are involved, relativistic effects are ignored and the system dynamics are given by solution to the time-dependent Schrödinger equation (2.15). For convenience all equations are given in atomic units with $\hbar = m_e = e = 1/(4\pi\epsilon_0) = 1$ and t is used throughout to represent time.

2.2. Theory

2.2.1. The Qubit

The qubit modeled in this work is based on the single-electron lateral coupled DQDs experimentally implemented by Petta et al. [26]. These are constructed from a GaAs/AlGaAs heterostructure containing a two-dimensional electron gas (2DEG) 100 nm below the surface that is controlled by Ti/Au top gates. Due to the strong vertical confinement of the system,

the qubit can be modeled in two-dimensions (x_1, y_1) with the Hamiltonian for the isolated qubit $\widehat{H}_q$ given by

$$\widehat{H}_q = -\frac{1}{2m^*}\nabla^2_{x_1,y_1} + V_q(x_1, y_1), \tag{2.1}$$

where $V_q(x_1, y_1)$ is the confinement potential. This low-energy confining potential is given to good accuracy by the parabolic potential [27]:

$$V_q(x_1, y_1) = \frac{1}{2}m^*\omega_0^2 \min\left\{x_1^2 + \left(y_1 - \frac{d}{2}\right)^2, x_1^2 + \left(y_1 + \frac{d}{2}\right)^2\right\}, \tag{2.2}$$

where ω_0 is the confining trap frequency, with $\hbar\omega_0 = 1\,\text{meV}$, and $d = 250\,\text{nm}$ is the interdot separation.

To describe the initial state of the isolated qubit electron a two-dimensional wavefunction $\Psi_q(x_1, y_1, t = 0) \equiv \Psi_q(x_1, y_1)$ is used. This wavefunction is expanded into a linear combination of the single-electron energy eigenstates $\varphi_i(x_1, y_1)$ that are solutions of the time-independent Schrödinger equation:

$$\widehat{H}_q\varphi_i(x_1, y_1) = \mathcal{E}_i\varphi_i(x_1, y_1), \tag{2.3}$$

where $\mathcal{E}_i$ is the energy eigenvalue corresponding to the electron state φ_i. The localized computational basis states, $|0\rangle$ and $|1\rangle$, are given by the two-dimensional Gaussian wave functions:

$$\begin{aligned} |0\rangle &= \frac{1}{\sqrt{\pi}\omega_q}\exp\left(-\frac{x_1^2 + (y_1 + y_0)^2}{2\omega_q^2}\right), \\ |1\rangle &= \frac{1}{\sqrt{\pi}\omega_q}\exp\left(-\frac{x_1^2 + (y_1 - y_0)^2}{2\omega_q^2}\right) \end{aligned} \tag{2.4}$$

with $\omega_q = 33.8\,\text{nm}$ and $y_0 = 125.0\,\text{nm}$. These states are then projected onto the two lowest eigenstates as

$$\begin{aligned} |0\rangle &= f_1\varphi_1 + f_2\varphi_2, \\ |1\rangle &= g_1\varphi_1 + g_2\varphi_2, \end{aligned} \tag{2.5}$$

where $f_i = \langle 0 \mid \varphi_i\rangle$ and $g_i = \langle 1 \mid \varphi_i\rangle$. The initial state of the qubit is then represented by

$$\begin{aligned} \Psi_q(x_1, y_1) &= c_0|0\rangle + c_1|1\rangle, \\ &= (c_0 f_1 + c_1 g_1)\varphi_1 \\ &\quad + (c_0 f_2 + c_1 g_2)\varphi_2. \end{aligned} \tag{2.6}$$

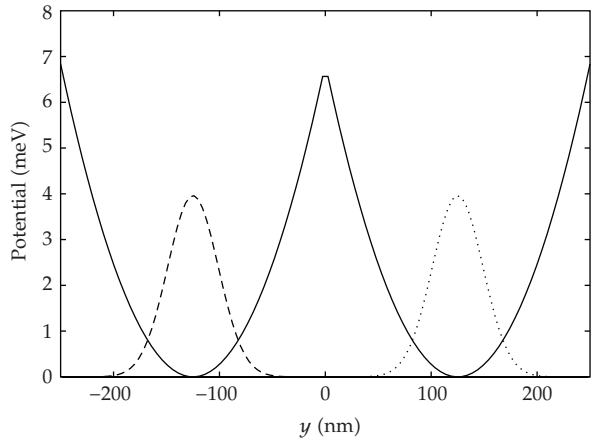

Figure 3: The qubit potential and electron probability density in the two localized computational basis states $|0\rangle$ and $|1\rangle$. The potential and probability densities are modeled in two-dimensions and symmetric about the x-axis; so only the values with $x_1 = 0$ nm are shown here.

The values of ω_q and y_0 were determined by optimization to ensure both zero overlap between the $|0\rangle$ and $|1\rangle$ basis states and that the electron state is essentially characterized by only the lowest two energy eigenstates. This ensures that the computational basis states used in the simulation are both *orthogonal* and *complete*, the probability densities of which can be seen in Figure 3. As the two lowest-energy eigenstates are not degenerate, the electron will oscillate about each basis state with characteristic time:

$$T = \frac{2\pi}{|\mathcal{E}_1 - \mathcal{E}_2|}, \tag{2.7}$$

which for the modeled confinement potential gives $T = 676$ nanoseconds. It is important to note that, due to this oscillation, the computational basis states are dynamic and so any general entanglement operation must take a significantly shorter time to be useful.

2.2.2. The Ballistic Electron

The ballistic electron being modeled is confined to a GaAs quantum wire containing double symmetric resonant tunneling barriers formed by two InAs slices embedded in the quantum wire heterostructure. Currently, GaAs quantum wires have been produced down to diameters of 5.99 nm [28] producing strong radial confinement and allowing the ballistic electron and resonant tunneling barriers to be effectively modeled in just one-dimension (x_2). InAs slices have been experimentally produced with variable widths down to less than 50 nm and with a maximum barrier potential of approximately 1.4 meV [29]. While the exact geometry of these potential barriers has yet to be established, similar experiments [30] with InP doped InAs wires have shown a good match to rectangular potential functions and so these are used here. The Hamiltonian for the isolated ballistic electron $\widehat{H}_w$ is then

$$\widehat{H}_w = -\frac{1}{2m^*}\nabla^2_{x_2} + V_w(x_2), \tag{2.8}$$

where $V_w(x_2)$ is the potential of the resonant tunneling barriers. This potential is modeled using

$$V_w(x_2) = \begin{cases} V_0, & \text{if } \dfrac{s}{2} \le |x_2| \le \dfrac{s}{2} + w, \\ 0, & \text{otherwise} \end{cases} \tag{2.9}$$

with $w = 50\,\text{nm}$ and $s = 90\,\text{nm}$ being the optimized width and separation of the barriers, respectively.

As initially the ballistic electron experiences no interactions with the qubit electron, its isolated wavefunction $\Psi_w(x_2, t = 0) \equiv \Psi_w(x_2)$ is described by the one-dimensional Gaussian wave packet:

$$\begin{aligned} \Psi_w(x_2) = \left(\frac{1}{\sqrt{\pi}\omega_w}\right)^{1/2} \exp\left(-\frac{(x_2 - x_0)^2}{2\omega_w^2}\right) \\ \times \exp\left(\imath p_0 (x_2 - x_0)\right), \end{aligned} \tag{2.10}$$

where p_0 is the initial momentum, $x_0 = -20\,\mu\text{m}$ is the initial position of the electron, and $\omega_w \equiv \sqrt{2}\Delta x$ is the uncertainty in the position. The limit of this uncertainty is calculated using the Heisenberg relation:

$$\Delta E \Delta x \ge \frac{1}{2m^*} p_0 = \sqrt{\frac{E_0}{2m^*}}, \tag{2.11}$$

where ΔE is the uncertainty in energy of the electron and $E_0 = p_0^2/(2m^*)$ is its initial energy. The uncertainty in position is therefore determined by the energy uncertainty of the single-electron source. Single-electron sources have been produced that can generate ballistic electrons on sub-nanosecond time-scales [24]. By taking the uncertainty in the generation time of these electrons to be of the same order, $\Delta t \approx 1\,\text{ns}$, and using Heisenberg's uncertainty principal, $\Delta E \Delta t \ge \hbar$, this gives an energy uncertainty of $\Delta E \ge 0.66\,\mu\text{eV}$. As the ballistic energies being considered here are of the order of meV, this uncertainty is conservatively represented by a fractional uncertainty of $\Delta E/E_0 \equiv \alpha = 1\%$. The uncertainty in position is then given by

$$\Delta x \ge \sqrt{\frac{E_0}{2m^*(\Delta E)^2}} = \frac{1}{\alpha p_0}. \tag{2.12}$$

2.2.3. Total System

To simulate the total system, the electrons in the qubit and quantum wire are described by the three-dimensional joint wavefunction $\Psi(x_1, y_1, x_2, t) \equiv \Psi$ where x_1 and y_1 represent

the position of the electron in the qubit, x_2 represents the position of the electron in the quantum wire, and t the time. The total Hamiltonian of the system $\widehat{H}_{\text{total}}$ is given by

$$\widehat{H}_{\text{total}} = \widehat{H}_q + \widehat{H}_w + \widehat{H}_{\text{int}}, \tag{2.13}$$

where $\widehat{H}_q$ is the Hamiltonian of the isolated qubit given by (2.1), $\widehat{H}_w$ is the Hamiltonian of the isolated ballistic electron given by (2.8), and $\widehat{H}_{\text{int}}$ is the Hamiltonian describing the Coulombic interaction acting on the combined Hilbert space of the two electrons given by

$$\widehat{H}_{\text{int}} = \frac{1}{\epsilon\sqrt{(x_1 - x_2)^2 + (y_1 - d)^2 + z^2}}, \tag{2.14}$$

where $d = 125\,\text{nm}$ is the distance between the quantum wire and the centre of the qubit and $z = 101\,\text{nm}$ is the vertical displacement of the quantum wire from the plane of the qubit. The values for d and z were fixed during the optimization to ensure the maximum interaction between the qubit and ballistic electrons. The value of z also includes a hypothetical 1 nm insulating layer to protect against possible charge leakage from the quantum wire.

The dynamics of the system are governed by the time-dependent Schrödinger equation:

$$\imath\frac{\partial\Psi}{\partial t} = \widehat{H}_{\text{total}}\Psi. \tag{2.15}$$

As the total Hamiltonian is time-independent, the system wavefunction $\Psi(\Delta t)$ at time Δt is given by

$$\Psi(\Delta t) = \exp\left(-\imath\widehat{H}_{\text{total}}\Delta t\right)\Psi_0 = \widehat{U}\Psi_0, \tag{2.16}$$

where $\Psi_0 \equiv \Psi(t = 0)$ is the system wavefunction at some arbitrary starting time, and $\widehat{U} \equiv \exp(-\imath\widehat{H}_{\text{total}}\Delta t)$ is the unitary evolution operator.

2.3. Numerical Simulation

The numerical techniques used in this simulation are based on those of Hines et al. [31] for the readout of a solid-state charge qubit. Initially the electrons are well separated, in two nonoverlapping Hilbert spaces, and so the initial system wavefunction is simply given by the product of their isolated wavefunctions:

$$\Psi_0 = \Psi_q(x_1, y_1)\Psi_w(x_2), \tag{2.17}$$

where $\Psi_q(x_1, y_1)$ and $\Psi_w(x_2)$ are the initial wavefunctions of the qubit and ballistic electrons given in (2.6) and (2.10), respectively. To represent the wavefunction numerically

the quantum wire is modeled using a one-dimensional grid of N_w points. The wire state is then projected onto the first N_q energy eigenstates of the qubit to give

$$\Psi_0 = \sum_{i=1}^{N_w} \sum_{j=1}^{N_q} b_{i,j} \psi_j(x_1, y_1), \tag{2.18}$$

where $b_{i,j}$ is the product of the ballistic electrons wavefunction at the ith point on the wire and the coefficient of the jth eigenstate of the qubit electron. The total system can then be modeled using only an $N_q \times N_w$ grid of complex numbers. To improve numerical accuracy the first eight eigenstates, $N_q = 8$, are considered with only the lowest two representing the computational basis states of the qubit.

Due to the complexity of the system being investigated, analytic solutions for the action of the evolution operator do not exist and so the Chebyshev-Fourier method [32] is used in the simulation. Briefly, this numerical method uses Fourier transforms to efficiently calculate derivatives as simple products in momentum space and approximates the evolution operator by using a Chebyshev polynomial expansion of the form

$$\begin{aligned} \widehat{U} = {} & \exp\left(-\imath \frac{(\mathcal{E}_u + \mathcal{E}_l)}{2} \Delta t\right) \\ & \times \sum_{i=0}^{M} a_i \left(\frac{(\mathcal{E}_u + \mathcal{E}_l)}{2} \Delta t\right) T_i\left(-\imath \widetilde{H}\right), \end{aligned} \tag{2.19}$$

where $\mathcal{E}_u$ and $\mathcal{E}_l$ are the upper and lower energies of the system, $\widetilde{H} = (2\widehat{H}_{\text{total}} - \mathcal{E}_u - \mathcal{E}_l)/(\mathcal{E}_u - \mathcal{E}_l)$ is the normalized Hamiltonian, T_i are the Chebyshev Polynomials, and a_i is the function

$$a_i(\alpha) = \begin{cases} J_0(\alpha), & \text{if } i = 0, \\ 2J_i(\alpha), & \text{if } i > 0 \end{cases} \tag{2.20}$$

with J_m being Bessel functions of the first kind. The advantage of this technique is that as the value of α grows larger than their order m, the Bessel functions fall to zero exponentially. Through a suitable choice of M, unitary solutions of the time-dependent Schrödinger equation (2.15) can be achieved up to an arbitrary accuracy. To then optimize the system parameters a standard multidimensional simplex minimization method was used [33].

3. Results and Discussion

The quantum mechanical phenomenon of coherent resonant tunneling describes the complete transmission of a ballistic electron through a set of barriers that is classically disallowed. It occurs when the incident energy of the ballistic electron closely matches one of the virtual energy eigenstates of the potential well formed by the barriers. At these specific energies the transmission probability is sharply peaked and the barriers are effectively "transparent" to the ballistic electron's wavefunction. The particular energies at which these peaks occur is determined solely by the geometry of the barrier potential and for

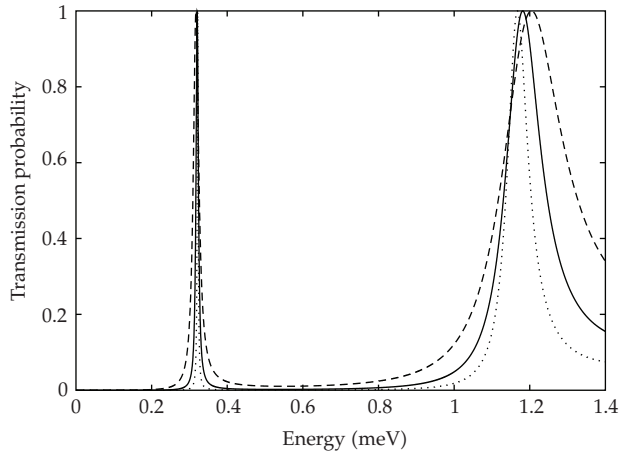

Figure 4: The calculated transmission probabilities for specific incident electron energies on a symmetric rectangular double barrier of height 1.4 meV and separation 90 nm with barrier widths 40 nm (dashed), 50 nm (solid), and 60 nm (dotted). Values were calculated analytically for an isolated ballistic electron.

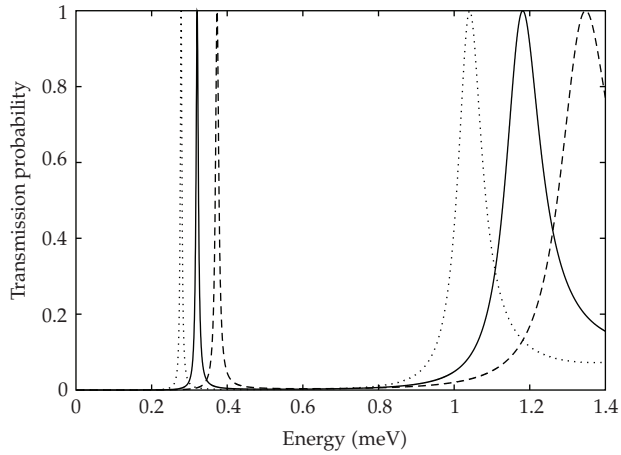

Figure 5: The calculated transmission probabilities for specific incident electron energies on a symmetric rectangular double barrier of height 1.4 meV and width 50 nm with barrier separations 80 nm (dashed), 90 nm (solid), and 100 nm (dotted). Values were calculated analytically for an isolated ballistic electron.

the one-dimensional case of an isolated ballistic electron and symmetric rectangular double barriers analytic solutions can be derived [34]. To demonstrate the sensitivity of the resonant tunneling system, transmission profiles were calculated using the analytic solution for varying barrier widths and separations and these can be seen in Figures 4 and 5, respectively. Due to the extreme sensitivity, small changes in the geometry of the barrier potential will cause large changes in the transmission probabilities of the ballistic electron. In our system, the localization of the qubit electron to one of the two basis states alters the strength of the Coulombic interaction with the ballistic electron and so affects the transmission probability causing entanglement.

It has been shown [35] that, while the particular mechanism of entanglement is unimportant, for any arbitrary quantum system to be used as a cluster state the localized entanglement between pairs of nearest neighbor qubits must be at a maximum. If this is not the case, then measurements on the individual qubits will result in the incomplete transfer of quantum information and computational errors will occur. For our scheme to create entanglement suitable for the generation of a cluster state in a *single step* it is necessary that after a tunneling event there is maximum entanglement between the electrons and that the state of the qubit is unchanged.

While there are many measures for quantifying the degree of entanglement, the most widely accepted, and that used here, is the concurrence or "entanglement of formation" [36]. For an arbitrary N qubit system $|\phi\rangle$ the concurrence $C(\phi)$ is given by

$$C(\phi) = \left|\langle\phi|\left(\sigma_y^1 \otimes \sigma_y^2 \otimes \cdots \sigma_y^N\right)|\phi^*\rangle\right|, \tag{3.1}$$

where $|\phi^*\rangle$ is the complex conjugate of $|\phi\rangle$ when expressed in a fixed basis, and σ_y^i are the Pauli matrices acting on the Hilbert space of the ith qubit in this basis. The concurrence is an entanglement monotone valued between 0 and 1, with $C(\phi) = 1$ for a maximally entangled state and $C(\phi) = 0$ if the state is separable. It has been shown [37, 38] that for two systems of arbitrary dimensions in a pure state this concurrence can be generalized to

$$C(\phi) = \sqrt{2\left[1 - \mathrm{tr}\left(\widetilde{\rho}_A^2\right)\right]}, \tag{3.2}$$

where $\widetilde{\rho}_A$ is the reduced density matrix of one of the subsystems. As initially both electrons are in pure states and the system evolution unitary, the final state of the system is pure and so the concurrence can be calculated using the reduced density matrix of the qubit.

To optimize the entanglement generated by a single resonant tunneling event, a simplex minimization method was used to alter the separation and width of the resonant tunneling barriers. For each set of barrier parameters, a series of simulations were run using the maximally mixed pure qubit state $|+\rangle \equiv (|0\rangle + |1\rangle)/\sqrt{2}$ over a range of ballistic electron energies. The total time for each simulation was dynamically set to ensure that the final position of the electrons was well separated and the concurrence for each calculated. The difference between unity and the maximum concurrence across the complete energy range was then used as the measure of fitness in the optimization. Using this technique, a maximum concurrence of 0.998 was achieved for a barrier width of 50 nm, separation of 90 nm, and with a ballistic electron energy of 1.585 meV.

Using the optimized system parameters, the probability of the ballistic electron becoming trapped was found to be negligible, the final state of the ballistic electron can be seen in Figure 6, and the tunneling was effectively elastic. Furthermore, the resonant tunneling event takes just 445 ps and so the qubit can be considered as static during entanglement (see (2.7)).

To investigate how resonant tunneling leads to this high level of entanglement, the transmission probabilities for the initial qubit states $|0\rangle$ and $|1\rangle$ were calculated using the optimized barrier parameters. The transmission profiles, as well as the corresponding concurrence values for an initial qubit state $|+\rangle$, are shown in Figure 7. As expected, there is a strong correlation between the difference in transmission probability of the two states and the concurrence of the system. Aside from the small secondary peak in the $|1\rangle$ profile at

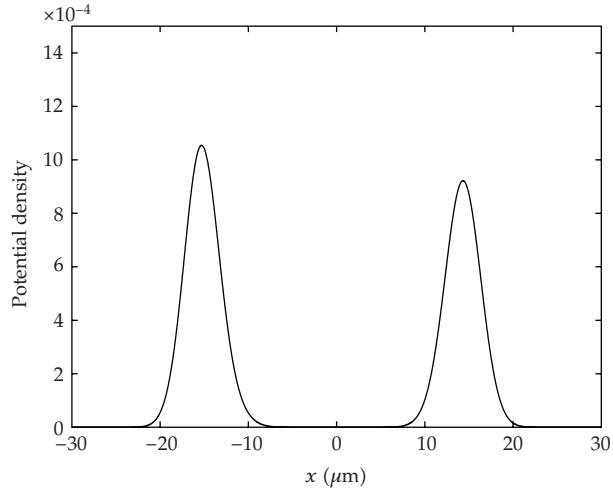

Figure 6: The probability density for the ballistic electron after entanglement ($t = 445\,\text{ps}$) for the qubit in initial state $|+\rangle \equiv (|0\rangle + |1\rangle)/\sqrt{2}$ using an initial energy of 1.585 meV and the optimised barrier parameters.

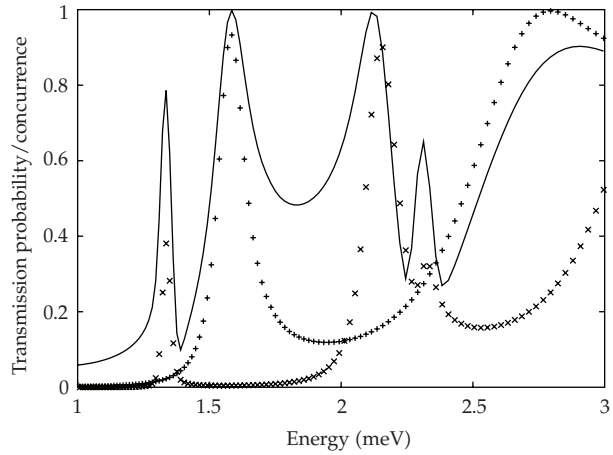

Figure 7: The concurrence of the system for the qubit in the $|+\rangle = (|0\rangle + |1\rangle)/\sqrt{2}$ state (solid line) and the transmission probabilities associated with the $|0\rangle$ (+) and $|1\rangle$ (×) qubit states over a range of ballistic electron energies and with optimized barrier parameters.

around 2.3 meV, both transmission profiles strongly resemble the analytic case for an isolated ballistic electron seen in Figure 5. This implies that resonant tunneling is being suppressed by the change in the ballistic electrons energy due to the Coulombic interaction with the qubit and not because of distortions in the potential of the resonant tunneling barriers themselves. The total potential experienced by the ballistic electron from both the resonant barriers and the overall Coulombic interaction of the qubit in each basis state can be seen in Figure 8. When the qubit is in the $|0\rangle$ state, there is very little change in the potential compared to the resonant barriers alone but there is an increase in the baseline energy of on average 0.41 meV (see Figure 8). Fitting the analytic solution to the calculated transmission peak gives good agreement across the whole probability profile with an increase in the baseline

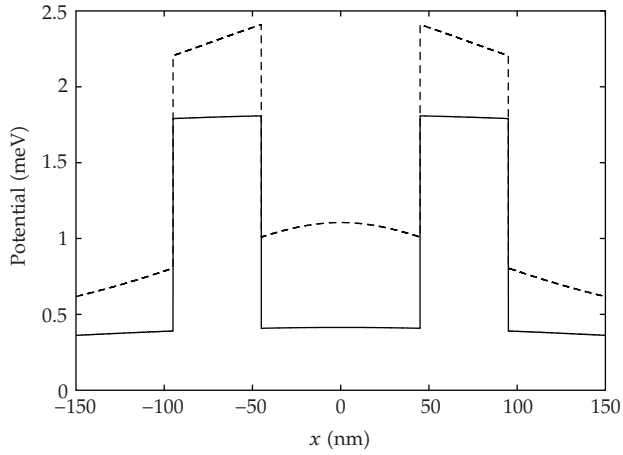

Figure 8: The total potential experienced by the ballistic electron when the qubit is in the initial states $|0\rangle$ (solid line) and $|1\rangle$ (dashed line).

energy of 0.40 meV. For the qubit in the $|1\rangle$ state the situation is not as straightforward as the shape of the potential is being noticeably distorted by the Coulombic interaction between the electrons (see Figure 8). Here the average increase in baseline energy is 0.99 meV compared to the value found by fitting the analytic solution of 0.97 meV. While the change in energy is similar, the analytic profile does not agree across the whole calculated probability profile and so distortions in the barrier shape do affect the transmission probabilities at certain ballistic energies.

To analyze the magnitude of this contribution to the entanglement, the mutual information about the initial state of the qubit Y given by the final state of the ballistic electron X was calculated using the standard formula:

$$I(X;Y) = \sum_{x\in X}\sum_{y\in Y} p(x,y)\log_2\left(\frac{p(x,y)}{p(x)p(y)}\right), \tag{3.3}$$

where x is the localization of the ballistic electron to either the left or right of the potential barrier and $y \in \{0,1\}$ is the qubit basis state. The mutual information for the initial qubit state $|+\rangle$ can be seen, with the corresponding concurrence, for a range of initial ballistic electron energies in Figure 9. As it ignores phase, the mutual information gives a good indication of the level of entanglement in the system due to transmission probabilities alone. From the graph it is apparent that, as expected, there is a strong correlation between the classical mutual information and concurrence with an equivalent maximum in the mutual information of 0.834. This suggests that while the primary mechanism for entanglement is the change in energy of the ballistic electron due to the Coulombic interaction, there is also a significant phase effect.

The generation of a cluster state requires not only maximal entanglement but also entanglement between all nearest neighboring qubits. If the resonant tunneling system is to be used to perform such entanglement in a *single step*, then it should not disrupt the state of the qubit and so allow multiple entanglement operations to be performed. From the reduced density matrix of the qubit, the probabilities after entanglement were found to be 0.50 and

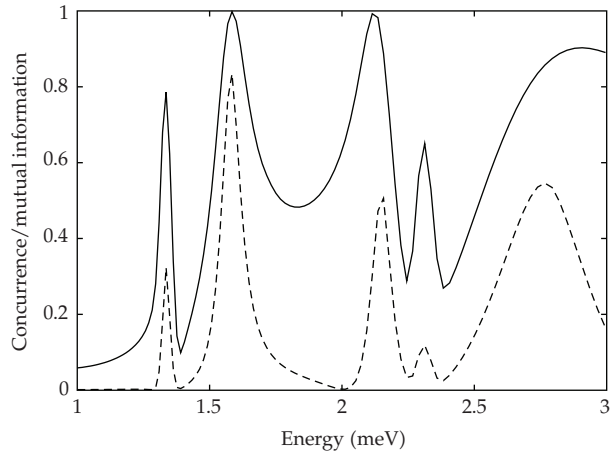

Figure 9: A comparison of the concurrence of the system (solid line) and the classical mutual information (dashed line) between the initial state of the qubit and the final position of the electron in the quantum wire over a range of initial ballistic electron energies and with optimized barrier parameters.

0.50 for the $|0\rangle$ and $|1\rangle$ basis states, respectively. This means that there is no change in the probability density of the qubit compared to its initial maximally mixed state $|+\rangle = (|0\rangle + |1\rangle)/\sqrt{2}$. Unlike the probability, the relative phase of the qubit basis states after entanglement is dependent on the basis state of the ballistic electron. As we are free to choose this basis, a state is selected that preserves the relative phase of the qubit. Simulations were then run using the optimized system parameters and maximally mixed initial qubit states with a range of relative and global phases. It was found that changes in the phase of the qubit do not affect the concurrence of the system and, by applying the selected ballistic electron basis state, that these phases were preserved after entanglement. This means that the resonant tunneling event does not introduce any relative phase in the state of the qubit and so the initial state of the qubit is completely preserved, as required.

To test the stability of the system, a series of simulations were run using small perturbations in each of the optimized parameters and the linear response of the concurrence calculated. It was found that a 1 nm change in the width and separation of the barriers gives an average change in the concurrence of -0.006 and -0.041, respectively and that a $1\,\mu$eV change in the initial energy of the ballistic electron gives an average change of -0.002.

4. Conclusions

In this paper we have provided a brief review of the theoretical foundations of cluster state quantum computation and how it evolved from the traditional model of digital computers. We also reported on numerical simulations of a solid-state system for generating controlled entanglement between a single-electron charge qubit and a ballistic electron using the suppression of coherent resonant tunneling in a quantum wire. It was found that a high level of entanglement could be achieved, with a concurrence of 0.998, and that the state of the qubit was unaffected by the process. The primary mechanism of entanglement was the difference in the transmission probabilities corresponding to the two localized basis states of the qubit. These differences occurred due to the Coulombic interaction between the electrons changing

the ballistic electron's energy which shifted the resonance peaks. If the ballistic electron can be used to entangle further qubits, then this scheme provides a viable method for the generation of cluster states.

The concurrence was found to be highly sensitive to the system parameters especially the barrier separation. This poses a significant limitation on any practical implementation of this scheme as it requires the precise fabrication of the resonant tunneling barriers and means that the system will be heavily affected by imperfections in their interface. The stability may be improved by using a different geometry for the barriers or a greater number but the effect this would have on the concurrence is unclear and more work needs to be done in this area. Furthermore, while the simulation was closely modeled on experimentally realizable components and treated the ballistic and qubit electrons and their interactions in detail, it did not include decoherence effects that would be present in a real system. This means that our results provide an idealized upper limit for the possible entanglement that such a practical implementation could produce.

Acknowledgments

The authors would like to thank N. Menicucci and C. Hines for valuable discussions. This work was supported by iVEC—The hub of advanced computing in Western Australia, The University of Western Australia, and the Australian Research Council.

References

[1] D. Deutsch, "Quantum theory, the church-turing principle and the universal quantum computer," *Proceedings of the Royal Society A*, vol. 400, no. 1818, pp. 97–117, 1985.

[2] R. Raussendorf and H. J. Briegel, "A one-way quantum computer," *Physical Review Letters*, vol. 86, no. 22, pp. 5188–5191, 2001.

[3] A. M. Turing, "On computable numbers, with an application to the entscheidungsproblem," *Proceedings of the London Mathematical Society*, vol. 42, pp. 230–265, 1936.

[4] R. P. Feynman, "Simulating physics with computers," *International Journal of Theoretical Physics*, vol. 21, no. 6-7, pp. 467–488, 1982.

[5] P. W. Shor, "Algorithms for quantum computation: discrete logarithms and factoring," in *Proceedings of the 35th Annual Symposium on Foundations of Computer Science*, pp. 124–134, IEEE Computer Society, Los Alamitos, Calif, USA, 1994.

[6] L. K. Grover, "From Schrödinger's equation to the quantum search algorithm," *American Journal of Physics*, vol. 69, no. 7, pp. 769–777, 2001.

[7] A. C.-C. Yao, "Quantum circuit complexity," in *Proceedings of the 34th Annual Symposium on the Foundations of Computer Science*, pp. 352–361, IEEE Computer Society, Los Alamitos, Calif, USA, 1993.

[8] D. P. DiVincenzo, "Two-bit gates are universal for quantum computation," *Physical Review A*, vol. 51, no. 2, pp. 1015–1022, 1995.

[9] A. Barenco, C. H. Bennett, R. Cleve, et al., "Elementary gates for quantum computation," *Physical Review A*, vol. 52, no. 5, pp. 3457–3467, 1995.

[10] R. Cleve, "An introduction to quantum complexity theory," in *Collected Papers on Quantum Computation and Quantum Information Theory*, C. Macchiavello, G. Palma, and A. Zeilinger, Eds., pp. 103–127, World Scientific, Singapore, 2000.

[11] R. Raussendorf, D. E. Browne, and H. J. Briegel, "Measurement-based quantum computation on cluster states," *Physical Review A*, vol. 68, no. 2, Article ID 022312, 2003.

[12] W. Dür and H.-J. Briegel, "Stability of macroscopic entanglement under decoherence," *Physical Review Letters*, vol. 92, no. 18, Article ID 180403, 2004.

[13] K. Kieling, T. Rudolph, and J. Eisert, "Percolation, renormalization, and quantum computing with nondeterministic gates," *Physical Review Letters*, vol. 99, no. 13, Article ID 130501, 2007.

[14] S. Y. Looi, L. Yu, V. Gheorghiu, and R. B. Griffiths, "Quantum-error-correcting codes using qudit graph states," *Physical Review A*, vol. 78, no. 4, Article ID 042303, 2008.
[15] M. A. Nielsen and C. M. Dawson, "Fault-tolerant quantum computation with cluster states," *Physical Review A*, vol. 71, no. 4, Article ID 042323, 26 pages, 2005.
[16] D. E. Browne and T. Rudolph, "Resource-efficient linear optical quantum computation," *Physical Review Letters*, vol. 95, no. 1, Article ID 010501, 4 pages, 2005.
[17] J.-Q. Li, G. Chen, and J.-Q. Liang, "One-step generation of cluster states in microwave cavity QED," *Physical Review A*, vol. 77, no. 1, Article ID 014304, 2 pages, 2008.
[18] P. A. Ivanov, N. V. Vitanov, and M. B. Plenio, "Creation of cluster states of trapped ions by collective addressing," *Physical Review A*, vol. 78, no. 1, Article ID 012323, 2008.
[19] T. P. Friesen and D. L. Feder, "One-way quantum computing in optical lattices with many-atom addressing," *Physical Review A*, vol. 78, no. 3, Article ID 032312, 2008.
[20] J. Q. You, X.-B. Wang, T. Tanamoto, and F. Nori, "Efficient one-step generation of large cluster states with solid-state circuits," *Physical Review A*, vol. 75, no. 5, Article ID 052319, 2007.
[21] G.-P. Guo, H. Zhang, T. Tu, and G.-C. Guo, "One-step preparation of cluster states in quantum-dot molecules," *Physical Review A*, vol. 75, no. 5, Article ID 050301, 2007.
[22] M. Borhani and D. Loss, "Cluster states from Heisenberg interactions," *Physical Review A*, vol. 71, no. 3, Article ID 034308, 4 pages, 2005.
[23] Y. S. Weinstein, C. S. Hellberg, and J. Levy, "Quantum-dot cluster-state computing with encoded qubits," *Physical Review A* , vol. 72, no. 2, Article ID 020304, 4 pages, 2005.
[24] G. Fève, A. Mahé, J.-M. Berroir, et al., "An on-demand coherent single-electron source," *Science*, vol. 316, no. 5828, pp. 1169–1172, 2007.
[25] B. Tanner, *Introduction to the Physics of Electrons in Solids*, Cambridge University Press, Cambridge, UK, 1995.
[26] J. R. Petta, A. C. Johnson, C. M. Marcus, M. P. Hanson, and A. C. Gossard, "Manipulation of a single charge in a double quantum dot," *Physical Review Letters*, vol. 93, no. 18, Article ID 186802, 4 pages, 2004.
[27] A. Wensauer, O. Steffens, M. Suhrke, and U. Rössler, "Laterally coupled few-electron quantum dots," *Physical Review B*, vol. 62, no. 4, pp. 2605–2613, 2000.
[28] H. Yu and W. E. Buhro, "Solution-liquid-solid growth of soluble GaAs nanowires," *Advanced Materials*, vol. 15, no. 5, pp. 416–419, 2003.
[29] N. Panev, A. I. Persson, N. Sköld, and L. Samuelson, "Sharp exciton emission from single InAs quantum dots in GaAs nanowires," *Applied Physics Letters*, vol. 83, no. 11, pp. 2238–2240, 2003.
[30] M. T. Björk, B. J. Ohlsson, C. Thelander, et al., "Nanowire resonant tunneling diodes," *Applied Physics Letters*, vol. 81, no. 23, pp. 4458–4460, 2002.
[31] C. Hines, K. Jacobs, and J. B. Wang, "Readout of solid-state charge qubits using a single-electron pump," *Journal of Physics A*, vol. 40, no. 27, pp. F609–F616, 2007.
[32] J. B. Wang and S. Midgley, "Quantum waveguide theory: a direct solution to the time-dependent Schrödinger equation," *Physical Review B*, vol. 60, no. 19, pp. 13668–13675, 1999.
[33] W. H. Press, B. P. Flannery, S. A. Teukolsky, and W. T. Vetterling, *Numerical Recipes in FORTRAN*, Cambridge University Press, Cambridge, UK, 2nd edition, 1992.
[34] B. Ricco and M. Y. Azbel, "Physics of resonant tunneling. The one-dimensional double-barrier case," *Physical Review B*, vol. 29, no. 4, pp. 1970–1981, 1984.
[35] M. van den Nest, A. Miyake, W. Dür, and H. J. Briegel, "Universal resources for measurement-based quantum computation," *Physical Review Letters*, vol. 97, no. 15, Article ID 150504, 2006.
[36] W. K. Wootters, "Entanglement of formation of an arbitrary state of two qubits," *Physical Review Letters*, vol. 80, no. 10, pp. 2245–2248, 1998.
[37] P. Rungta, V. Bužek, C. M. Caves, M. Hillery, and G. J. Milburn, "Universal state inversion and concurrence in arbitrary dimensions," *Physical Review A*, vol. 64, no. 4, Article ID 042315, 13 pages, 2001.
[38] Y.-C. Ou and H. Fan, "Bounds on negativity of superpositions," *Physical Review A*, vol. 76, no. 2, Article ID 022320, 2007.